Identification of hydro-meteorological drivers for low greenness events in Europe

Pauline Rivoire[1,2], Sonia Dupuis[3,4], Antoine Guisan[1], Pascal Vittoz[1], and Daniela I.V. Domeisen[1,5]

[1]Institute of Earth Surface Dynamics, Faculty of Geosciences and Environment, University of Lausanne, Switzerland
[2]Laboratory of Cryospheric Sciences (CRYOS), School of Architecture, Civil and Environmental Engineering (ENAC), École Polytechnique Fédérale de Lausanne (EPFL), Lausanne, Switzerland
[3]Institute of Geography, University of Bern, Switzerland
[4]Oeschger Centre for Climate Change Research, University of Bern, Switzerland
[5]Institute for Atmospheric and Climate Science, ETH Zurich, Zurich, Switzerland

Correspondence: Pauline Rivoire (pauline.rivoire@unil.ch)

Abstract. Extreme hydro-meteorological events can have a substantial impact on vegetation and ecosystems. In particular, with heatwaves and droughts projected to become more frequent due to climate change, understanding their effects on forests is crucial. The goal of our study is to find the most relevant predictors for forest damage in Europe at monthly to annual timescales. Using a Random Forest approach, we pinpoint hydro-meteorological conditions associated with low normalized

5   difference vegetation index (NDVI) events. We train the model using the NDVI from the Advanced Very High Resolution Radiometers (AVHRR) as the predictand, and a range of variables from the ERA5 and ERA5-Land reanalysis as hydro-meteorological predictors. These predictors include maximum temperature at 2 meters and dewpoint temperature, precipitation, surface latent heat flux, and soil moisture up to 18 months before the observed damage. The random forest model exhibits a high prediction skill over most gridpoints in Europe, with a critical success index greater than 0.75 for 67% of gridpoints.

10   Notably, warm and dry conditions in spring and early summer emerge as essential predictors. Additionally, we emphasize a longer-term relationship between hydro-meteorological conditions and forest damage. For instance, low dewpoint temperatures one year before the studied summer impact broad-leaved forests, while soil moisture during the preceding autumn influences low greenness events in coniferous forests, albeit with location-specific variations.

1 Introduction

15   Forests cover about 202 millions hectares in Europe (FAO, 2020), or about 32 % of its land area. It is now well understood that forests offer essential ecosystem services such as soil conservation and fertility, water storage, regulation, and purification, protection against landslides and avalanches, air cleaning, wood production, habitat for a high biodiversity, without forgetting their aesthetic, spiritual and recreational value (Jenkins and Schaap, 2018). Due to climate change favoring diseases and pests (Pureswaran et al., 2018), the death of trees over large forest areas as observed in recent years (i.e., forest dieback; Senf et al.,

20   2020; Adams et al., 2017) is likely to have significant consequences on the economy and society, including loss of wood quality, increased erosion, and flood risk, and degradation of landscape quality.

The health of trees and forests strongly depends on hydro-meteorological conditions. In particular, dry and hot conditions can be highly detrimental to forests (Brodribb et al., 2020). Droughts can lead to early leaf senescence, parasite infestations, higher fire risk, loss of canopy greenness, and enhanced crown and tree mortality (Brun et al., 2020; Frei et al., 2022; Mariën et al., 2021; Sperlich et al., 2015). Large and persistent deviations from normal conditions can impact the photosynthesis capacity and carbon intake (Hinckley et al., 1979; Sperlich et al., 2015). In addition, consecutive dry years can lead to a larger impact on forests than the individual impact of dry years, due to the increased vulnerability of the trees (Anderegg et al., 2015). Adverse hot and dry conditions causing forest damage are expected to become more frequent and more intense under climate change (IPCC, 2022). Moreover, Meier et al. (2021) showed that a longer growing season amplified drought effects due to earlier spring leaf unfolding.

An improved understanding of the hydro-meteorological drivers of forest damage and their relative importance on different timescales will benefit the potential for advance prediction of such damage. In turn, successful predictions of forest health would benefit the design and implementation of efficient protection measures. Such predictions are expected to be possible due to a range of drivers affecting the greenness of trees and acting on timescales of weeks to years. For example, precipitation and temperature conditions strongly influence forest health. Hermann et al. (2023) showed that, in Europe, reduced summer forest greenness is preceded by positive temperature anomalies and negative precipitation anomalies in spring. Adverse air and soil humidity conditions can also impact tree health, such as anomalies in vapor-pressure deficit (Grossiord et al., 2020; McDowell et al., 2022), potential evapotranspiration (Young et al., 2017), or soil moisture (Alavi, 2002).

Preventive actions can be taken before conditions trigger forest vulnerability. Examples include forest-fire prevention (Ferreira et al., 2015), sanitation logging, and predation using long-legged flies (*Medetera* spp.) to prevent spruce bark beetle (*Ips typographus*) infestations (Jan Weslien et al., 2024). On longer timescales of years to decades, a good understanding of forest susceptibility to meteorological conditions may help managers target regions with the highest priority to adaptation and select tree species that are better adapted to future conditions. In this context, we choose to study hydro-meteorological variables available from operational forecasts covering the subseasonal-to-seasonal (S2S) timescale. For example, the ECMWF subseasonal forecasts cover timescales up to 1.5 months in advance and have been used to predict extreme events (Domeisen et al., 2022) and their surface impacts (White et al., 2022) from a range of atmospheric conditions. In particular, the ECMWF S2S forecast model includes the following hydro-meteorological variables: 2-meter temperature, precipitation, dew-point temperature (as an estimate of air humidity), soil moisture with soil-water equivalent, and surface latent heat flux (as an estimate of potential evapotranspiration). Our analysis establishes a link between these hydro-meteorological variables and forest health, allowing forest practitioners to anticipate adverse conditions based on the ECMWF S2S forecast.

Machine learning can leverage extensive data to predict vegetation states based on weather and climate conditions (John Nay and Gilligan, 2018; Vogel et al., 2021; Kladny et al., 2024). In this work, we introduce an automated procedure to identify and quantify adverse hydro-meteorological S2S conditions for forests in Europe. We employ a random forest (RF) classification to predict low greenness events. The RF model is a non-parametric algorithm, based on decision trees. Therefore, the RF model has the advantage of being both flexible and easily interpretable. From a large set of potential predictors, we pinpoint crucial, location-specific periods and variables impacting European forests.

2 Data

2.1 NDVI data

Forest damage can be assessed using a range of indices, including vegetation indices based on satellite Earth observation, for a
60   direct assessment of vegetation stress over large areas (Bannari et al., 1995; Zeng et al., 2022). We employ here the normalized
difference vegetation index (NDVI, Kriegler et al., 1969; Rouse et al., 1974), a measure of vegetation greenness, widely used to
monitor the health of forests (Zhou et al., 2003; Pettorelli et al., 2005; Buras et al., 2021; Rumpf et al., 2022). When measured
over large areas compared to the size of an individual tree, the NDVI captures forest vitality losses, resulting from reduced
canopy greenness or tree mortality.

65   The NDVI is defined by $\mathrm{NDVI} = \frac{\mathrm{NIR\text{-}red}}{\mathrm{NIR + red}}$, where NIR and red represent the spectral reflectance measurements in the near-
infrared and red portion of the electromagnetic spectrum, respectively. The NDVI values corresponding to vegetation are
typically between 0 and 1, with values close to one indicating very green, dense, and healthy vegetation. Lower NDVI values
indicate either sparse vegetation or browning of the vegetation, a visible sign that the plants are undergoing stress or damage.

We use the daily NDVI dataset generated from the Advanced Very High Resolution Radiometers (AVHRR) onboard the
70   National Oceanic and Atmospheric Administration's (NOAA) satellites NOAA-6 to -19, and the EUMETSAT MetOp satel-
lites series (MetOp1, MetOp2 and MetOp3) Local Area Coverage (LAC) dataset archived at University of Bern, Switzerland
(Dupuis et al., 2024; Barben et al., 2024; Weber et al., 2021). The advantage of the AVHRR dataset over Europe is the long
period of data availability, from 1981 to 2022 (for our analysis), as well as the fine spatial resolution of about $0.01°\mathrm{W} \times 0.01°\mathrm{N}$
(effective footprint of approximately 1 km^2).

75   Changes in sensor versions (AVHRR/1-3) require a homogenization of the spectral response function before combining the
data of the different sensors. This processing is performed with a polynomial correction with NOAA-9 as a reference (see,
Trishchenko et al., 2002; Trishchenko, 2009; Fontana et al., 2009). We discarded NOAA-15 due to poor data quality and
MetOp3 due to the absence of specific correction coefficients for the spectral response function (see Fig. A1 in the appendix
for the time distribution of the satellites used).

80   We average the daily AVHRR NDVI to a 10-day composited dataset, that has the advantage of offering a gap-free and
consistent dataset. In the present case, three NDVI scenes are available each month. The scenes cover the time periods from
the 1st to the 10th day, the 11th day to the 21st and finally from the 21st day until the end of the month, respectively. In
the following, a composite refers to a 10-day averaged NDVI. The AVHRR-NDVI dataset comprises different quality flags
linking to cloud probability and satellite viewing angle. We discard data points with too high image uncertainty due to clouds
85   or satellite viewing angles (see details in the appendix, Sec.A). To obtain a single time series out of the observations from the
different satellites, we retain for a given composite and a given pixel the daily maximum of NDVI for each satellite available
for a given composite.

2.2 From NDVI to binary forest damage

We summarize the vegetation greenness information brought by the NDVI with the binary damage data to encapsulate the
state of the forest during summer (July-August), at the same grid resolution as the drivers ($0.1°$, see section 2.3). Fig. B1 in
the appendix displays the entire time series of binary forest damage. In a nutshell, a $0.1°$ gridpoint (GP) is said to experience
a low-greenness event, if more than 80% of the forest pixels (within this given GP) experience a negative anomaly of NDVI,
during more than 80% of the July-August composites. More specifically, the binary forest damage, Y_t (for $t = 1981, \ldots, 2022$)
is defined through three steps, following the method of Hermann et al. (2023):

1. Monthly linear detrending of the composite NDVI time series (Bastos et al., 2017);

2. Computation of NDVI'$_j$, the NDVI anomalies for every composite j in July-August. NDVI'$_j$ is defined by: NDVI'$_j = \frac{\mathrm{NDVI}_j - median_{\mathrm{JA}}(\mathrm{NDVI})}{IQR_{\mathrm{JA}}(\mathrm{NDVI})}$, with NDVI$_j$ the detrended NDVI on composite j, $median_{\mathrm{JA}}(\mathrm{NDVI})$ the median of July-August detrended NDVI and IQR_{JA} the inter-quartile range of July-August detrended NDVI;

3. Upscaling of the AVHRR NDVI grid on the ERA5 land grid (from $0.01°$ to $0.1°$) and binarization to anomalies for the whole summer, with the following rule:
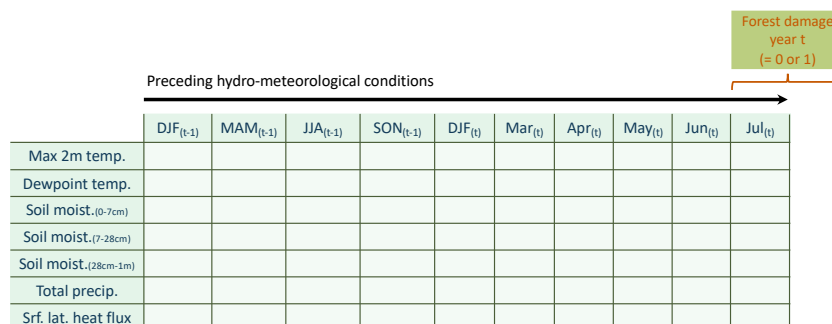
$$
Y_t = \begin{cases} 1 & \text{if } > 80\% \text{ of the forest GPs experience} \geq 5 \text{ composites with NDVI'} < 0 \\ \\ 0 & \text{otherwise} \end{cases}
$$

for a given year t. The criterion "≥ 5 composites with NDVI' < 0" implies "≥ 5 composites out of 6 with NDVI' < 0",
as the total number of 10-day composites in July-August is 6.

We only consider GPs (on the $0.1°{\times}0.1°$ grid) with forest coverage of at least 10%. The forest coverage and forest type
(broad-leaved, coniferous, mixed forests, see Fig. D1) are extracted from the CORINE (Coordination of Information on the
Environment) Land Cover for the reference year 2018 (EEA, 2020).

During step 3., we discard forest GPs with more than one missing data point per summer (out of 6 composites). This
requirement ensures an actual extremeness of the summers, with at least 5 composites out of 6 presenting negative NDVI
anomalies ($Y_t = 1$ in step 3). Due to a low NDVI quality in 1988, this year had to be discarded for all GPs in Europe (hence
the absence of 1988 in Fig. B1).

Although Hermann et al. (2023) relied on MODIS NDVI observations (Didan, 2015), we observe consistent patterns of low-
greenness events over Europe between 2002 and 2022, by comparing Fig. C1. in their analysis and Fig. B1 in our study. These
coherent patterns advocate for using AVHRR data for extended temporal coverage. In addition, AVHRR offers a finer spatial
resolution than MODIS (approximately 100m versus 250m). The resolution of the NDVI dataset can impact the significance of
the results as demonstrated by Rumpf et al. (2022), who found 77% of pixels with a greening trend using Landsat, compared
to 56% with MODIS in Choler et al. (2021).

	DJF$_{(t-1)}$	MAM$_{(t-1)}$	JJA$_{(t-1)}$	SON$_{(t-1)}$	DJF$_{(t)}$	Mar$_{(t)}$	Apr$_{(t)}$	May$_{(t)}$	Jun$_{(t)}$	Jul$_{(t)}$
Max 2m temp.										
Dewpoint temp.										
Soil moist.$_{(0-7cm)}$										
Soil moist.$_{(7-28cm)}$										
Soil moist.$_{(28cm-1m)}$										
Total precip.										
Srf. lat. heat flux										

Preceding hydro-meteorological conditions

Forest damage year t (= 0 or 1)

Table 1. 10 variables and 7 time-steps considered as potential drivers. Each of the 70 cells is a predictor for the binary forest damage in summer of the year t.

2.3 Hydro-meteorological predictors

To capture potential adverse conditions for forests (Hermann et al., 2023; Grossiord et al., 2020; Young et al., 2017; Alavi, 2002), we select the following seven hydro-meteorological variables as potential drivers for low-greenness events: maximum 2-m temperature, maximum 2-m dewpoint temperature, soil moisture at depths 0-7 cm, 7-28 cm, 28-100 cm, total precipitation, and surface latent heat flux. We extract these seven variables for the period 1980-2022 from the ERA5 and ERA5-Land reanalysis datasets for (Hersbach et al., 2019; Muñoz-Sabater et al., 2021). Reanalysis data offers dynamically consistent variables with a large, uniform spatio-temporal coverage. For temperature, dew-point temperature, and soil moisture, we use ERA5-Land data on a 0.1° resolution, and for total precipitation and surface-latent heat flux, we use ERA5 data on a 0.5° resolution.

We compute the variables' monthly mean anomalies between March and July of the same year of the studied summer (forest damage in July-August), and the seasonal mean anomalies up to 18 months before the studied summer (Table 1). For a given variable, the monthly (seasonal) mean anomaly is defined by $\frac{x - \bar{x}}{\sigma_x}$, where x is the monthly (seasonal) mean of the variable, $\bar{x}$ is the climatology –i.e. the monthly (seasonal) mean of the variable averaged over 1980-2022– and σ_x is the climatological standard deviation of the variable's mean (seasonal). We use seasonal anomalies (December-February, March-May, June-August, September-November), rather than monthly, for the preceding conditions anterior to 5 months before July-August, as only strongly anomalous conditions are expected to have a long-term lagged impact.

Each cell in Table 1 is used as a predictor for forest damage for a given year. With the term "predictor", we refer to a variable at a given time step. Consequently, there are 70 potential predictors in total.

2.4 Aggregating data for longer time series

135 The binary forest damage, our predictand, is a time series of 41 data points between 1981 and 2022, which is too short for a robust estimation of the statistical link between predictors and predictand. We therefore artificially create longer time series using the large amount of data available spatially. The 25 time series of GPs located in the same $0.5° \times 0.5°$ grid box are stacked temporally by assuming that the damage in neighboring GPs is driven by the same predictors (see Fig. C1 in the appendix). We thereby obtain longer times series, up to 1025 data points (25×41) for each sub-region. Note that 1025 is the maximum length,

140 which is obtained only if the 25 GPs are forest GPs (as defined in section 2.2), with a sufficient data quality for every summer (as specified in sections 2.1 and 2.2). For a robust statistical fitting, we discard stacked, balanced times series shorter than 80 datapoints.

3 Method

3.1 Random forest

145 A large number of predictors (70, see Section 2.3) are potential candidates to explain forest damage. To identify the most important predictors and their link to forest damage, we employ a random forest (RF) model (Breiman, 2001). The principle of a RF model is to compute a large number of decision trees, each fitted with a random sub-selection of the initial data, to assess the average link of each predictor with the predictand (binary forest damage here) and its importance compared to the others. We use 300 decision trees and 3 predictors per tree. These hyperparameters are found to be a good trade-off between

150 performance and computation time (not shown). We randomly divide the time series into a training subsample (75%) and a testing subsample (25%). The training data is used to both fit the RF model and calibrate the cutoff level of the RF output, to assign a probability of damage to a "0" or a "1", to compute the critical success index on the testing data (see the following section 3.2).

The years with forest damage represent extreme conditions and are rare by definition. For a majority of gridpoints (GPs),

155 less than 15 % of the years are "1"s (see Fig. B2 in the appendix). The rest of the years are "0"s, that is, normal years without relevant forest damage. For a higher performance of the RF, we force the impact data to be balanced by discarding "0" years in order to have the same amount (rounded up to ten) of "0"s and "1"s in the impact data. This random removal of years additionally breaks potential temporal autocorrelation induced by stacking time series temporally. In the end, we obtain a model for 1248 GPs over Europe.

160 The output of the RF function includes the mean decreased accuracy, a measure of the predictor's importance. The mean decreased accuracy of a given predictor quantifies the loss in predictive performance when this predictor is not included in the decision tree.

We use partial dependence analysis to interpret the influence of single variables (Friedman, 2001; RDocumentation, 2024). A partial dependence plot shows how the average probability of observing a specific outcome (e.g. forest damage) changes

165 with a single input variable. The mean probability is calculated across all observations for the other predictors. The partial dependence is plotted employing the following formula:

$$\tilde{f}(x) = \frac{1}{2n} \sum_{i=1}^{n} \left(\log \left(\frac{p_1(x, x_{iC})}{1 - p_1(x, x_{iC})} \right) \right),$$

where x is the value of the predictor for which partial dependence is calculated, p_1 is the proportion of votes for the class "1" (forest damage), and x_{iC} are all the other predictors in the training data and n is the length of the training data. $\tilde{f}$ is calculated

170 for all the values of x in the training data. A high $\tilde{f}(x)$ indicates that the value x for the chosen predictor is associated with a high probability of forest damage.

3.2 Performance

We measure the skill of the RF model on the testing data with the critical success index (CSI; Schaefer, 1990). The CSI is defined as $CSI = \frac{TP}{TP+FP+FN}$, where TP is the number of true positives (successfully predicted and observed low greenness

175   event, $Y_t = 1$), FP is the number of false positives (i.e. false alarm, the model wrongly predicted a low greenness event) and FN is the number of false negatives (i.e. missed events, the model erroneously predicted $Y_t = 0$). The CSI focuses on the predictive skill of the low greenness events, which is the quantity of interest in our analysis. The accurately predicted normal years ($Y_t = 0$) are not considered. The CSI varies between 0 and 1, the higher the better. A CSI of 0.5 means that the model predicted as many TP as the sum of FP and FN.

180   To assess the performance over all cut-off levels (see section 3.1), we additionally compute the AUC, that is the area under the ROC curve (Swets, 1988). The ROC (receiver operating characteristic) curve displays the true positive rate versus the false positive rate, against all cutoff levels. The AUC varies between 0 and 1, with values of 0 to 0.5 meaning counterpredictions, value of 0.5 meaning predictions not different than random, and values higher than 0.5 indicating increasingly good predictions.

3.3   LASSO regression

185   We additionally run a LASSO logistic regression (Tibshirani, 1996), with the same predictors, predictand, training, and testing data as for the RF. Vogel et al. (2021) demonstrated that the LASSO regression shows good performance in identifying meteorological drivers of extreme events (low wheat yield, in their study). We therefore employ the LASSO logistic regression as a benchmark for the predictive skill. The penalty factor on the coefficients norm (λ_{1se} in Vogel et al., 2021) is obtained with a 10-fold cross-validation.
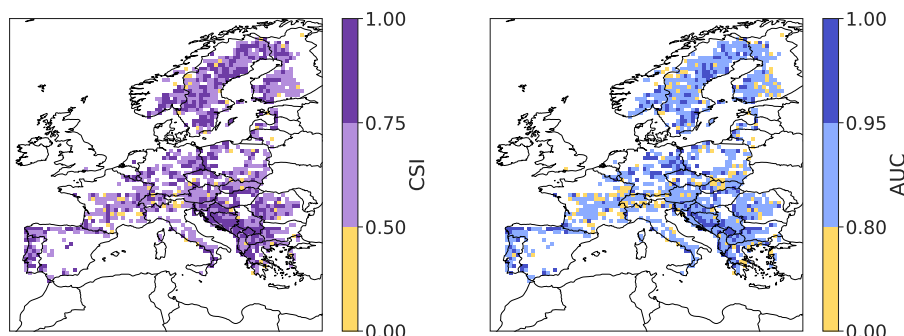
Figure 1. (a) CSI and (b) AUC (as defined in section 3.2) of the random forest model, evaluated for the training dataset.

4 Results

4.1 Performance

As a first step, we evaluate the performance of the random forest (RF) classification model at predicting low-greenness events from the hydro-meteorological predictors (i.e. from the aforementioned variables and time periods, Table 1). The RF model exhibits excellent predictive performance for forest damage over Europe (see Fig. 1): 99% of the GPs have a CSI greater than 0.5 (Fig. 1(a)). In other words, for 99% of the gridpoints (GPs), the model run on the testing data predicts at least as many true positives (TP) as false positives (FP) and false negatives (FN) together. 67% of the GPs have a CSI greater than 0.75 (i.e. at least three times as many TP as FP and FN together). The AUC also indicates a good performance, with 83% of the GPs having an AUC greater than 0.9. The high AUC proves that the good performance does not depend on the cutoff level. In other words, the true positive rate is much higher than the false positive rate for all cutoff levels between 0 and 1.

There is no specific region showing a lower skill. The Balkans and Sweden exhibit particularly large areas of high skill, for both metrics.

When aggregating GPs temporally to obtain longer time series, we formulated the hypothesis that the neighboring $0.1° \times 0.1°$ GPs in a $0.5° \times 0.5°$ grid box are driven by the same predictors. The high skill of the RF, in terms of both CSI and AUC, confirms that this hypothesis is sound.

In comparison with RF, the LASSO model exhibits a lower CSI for 80% of the GPs, and a lower AUC for 86% of the GPs (not shown). Only 92% of the GPs exhibit a CSI greater than 0.5 for LASSO (99% for RF). Regarding the AUC, 52% of the GPs attain an AUC above 0.9 with LASSO (83% for RF). An advantage of the LASSO logistic regression is the simple, linear link between predictors and predictand. This simplified link is outperformed by RF, allowing for flexible non-linear relationships between predictors and predictand.

4.2 Important drivers of forest damage

4.2.1 Example for two gridpoints

As an introduction of the important output of the RF model, we display the results for two GPs in Europe (their location is displayed in red in Fig. D1): one in a broad-leaved forest in France and one in a coniferous forest in Sweden.

For the broad-leaved GP in the Jura forest in France (Fig. 2, gridpoint (A)), the most important variables include dew point temperature, max 2-m temperature, soil moisture between 0 and 21 cm, and total precipitation (left panel). The important time periods are spring and early summer of the same year when the damage occurs, as well as summer and spring conditions one year preceding forest damage, for soil moisture and temperature. The 3 most important predictors are maximum dew point temperature in March, maximum 2-m temperature in June and soil moisture (7-21cm) during the preceding summer. Positive anomalies of dewpoint temperature in March are largely associated with forest damage, indicating that moist conditions in early spring are adverse for the forest at this GP. Warm conditions in June increase the likelihood of forest damage, as indicated by the partial dependence of maximum 2-m temperature. Negative soil moisture anomalies in summer the year before are associated with a higher probability of forest damage.

For the coniferous GP in Sweden (Fig. 2, GP (B)), the low greenness events are largely explained by the hydro-meteorological conditions during the preceding year, especially the conditions in spring, autumn, and summer. Soil moisture between 0 and 21 cm is particularly important (6 predictors out of the 10 most important). The link between total precipitation in spring the year before and forest damage is non-linear: both positive and negative anomalies are associated with a higher probability of damage, although the impact of dry conditions is stronger. The same non-linear signal is observed for soil moisture during the same period. However, only small negative anomalies of soil moisture in autumn are associated with forest damage.

4.2.2 Results over Europe

To summarize the model results for all GPs over Europe, we display, for each predictor, the percentage of GPs over Europe that selected this predictor as one of the ten most important predictors in the RF model (Fig. 3(A)). The time period with the strongest influence on forest damage is spring and early summer right before the studied summer, especially for maximum 2-m temperature and soil moisture. In particular, the most selected predictor is maximum 2-m temperature in June, with 39% of the GPs retaining this predictor as one of the 10 most important ones. Additionally, 22% (resp. 19%) of the GPs retained total precipitation in May (resp. April) as an important predictor. We observe a small signal of long-term impact of spring and autumn the year before. During the previous year, maximum 2-m temperature and dew point temperature are among the top 10 predictors for 23% and 20% of the GPs, respectively.

As forests are quite heterogeneous in Europe (Ozenda, 1994; Leuschner and Ellenberg, 2017; Lindner et al., 2014), we separate the analysis into broad-leaved and coniferous forests. Most of the broad-leaved forest GPs are located in the southern half of Europe, while most of the coniferous forests are located in the northern half (see Fig D1). This separation into tree types therefore roughly divides Europe into a northern and a southern area. Although the broad-leaved/coniferous separation discards many GPs that are classified as mixed forests, it allows for a clear identification of important variables and time periods.

Gridpoint **(A)** in France (6.5°E, 47.5°N), broad-leaved forest
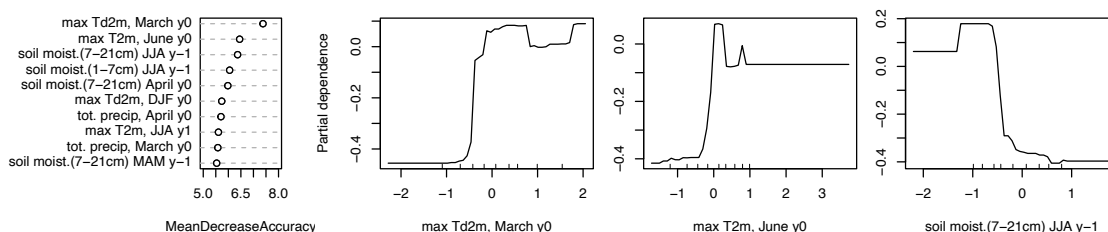
Gridpoint **(B)** Sweden (12.5°E, 59°N), coniferous forest
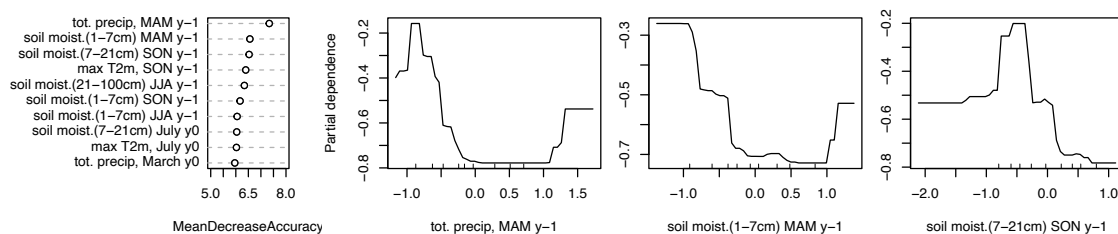
Figure 2. First column: 10 most important predictors (y-axis), i.e. predictors with the largest mean decrease accuracy (x-axis) for a gridpoint in broad-leaved forests in France (A) and a gridpoint in coniferous forests in Sweden (B) (location indicated on Fig. 1). Second, third, and fourth column: partial dependence of the forest damage (y-axis) with the predictor's anomalies (x-axis), for the 3 most important predictors.

For the broad-leaved forests, the most selected predictor is maximum 2-m temperature in June of the year of the damage (126 GPs, i.e. 48% of the broad-leaved GP, Fig 3 (B)). Except for two GPs, the ensemble of partial dependence plots shows two
245 clear plateaus, separating negative and positive temperature anomalies, the latter being associated with forest damage (Fig. 4 (A), first panel). The same is true for the second most selected predictor, maximum 2-m temperature in May of the year of the damage (101 GPs, i.e. 38% of the broad-leaved GP, Fig. 4 (A), second panel). Soil moisture (7-100 cm) in May, June, and July, and total precipitation in March, May and June of the same year also play a role for 35% and 32% of the GPs, respectively (Fig 3 (B)). In addition, there is an influence of spring conditions one year before for 2-m temperature and dewpoint temperature
250 (for 28% and 27% of the GPs). Negative anomalies of dewpoint temperature, i.e. dry air conditions, correspond to a higher probability of forest damage, for 27% of the broad-leaved GPs (Fig. 4 (A), last panel). These partial dependence patterns for broad-leaved forest do not depend on the latitude of the GP (see colors in Fig. 4 (A)).

The spring and early summer conditions before the studied summer are important predictors for coniferous forest damage (Fig. 3 (C)). The most selected predictor is maximum 2-m temperature in July (109 GP, i.e. 36% of the GP), followed by
255 dewpoint temperature in the same month (31%), maximum temperature, and soil moisture (1-7 cm) in June (30 %) and total precipitation in March of the same year. We also observe an influence of conditions in preceding years, especially for soil mois-

ture in summer and autumn the year before (24%). Compared to broad-leaved forests, the link between important predictors and coniferous forest damage is more heterogeneous (Fig. 4 (B)). Surprisingly, some GPs at high latitudes show that negative anomalies of maximum 2-m temperature in July are associated with a higher probability of forest damage (see the blue lines in

260 the first panel of Fig. 4 (B)). For some forest GPs at lower latitudes, positive anomalies of maximum 2-m temperature in July correspond to a higher probability of damage than negative anomalies (see the black lines, first panel of Fig. 4 (B))). Negative anomalies of dew point temperature in July (i.e. dry conditions in July) are associated with a higher forest damage probability. The link with soil moisture in autumn the year before is non-linear for some GP and overall very dependent on the GP, making a generalization over the region tricky. However, there is a slight indication that negative soil moisture anomalies in the fall of

265 the previous year may be linked to a higher probability of forest damage.

Altogether, the sub-seasonal to seasonal conditions of temperature and soil moisture in spring and early summer are the most important features to explain summer forest damage in Europe. Temperature and moisture conditions in spring, summer, and autumn the year before play a smaller role. The more relevant captured conditions for low greenness events in broad-leaved forests are hot and dry, in spring and early summer (of the same year or the preceding year). Lower-than-average summer

270 temperatures are among the most adverse conditions for coniferous forests, with exceptions depending on the GP.
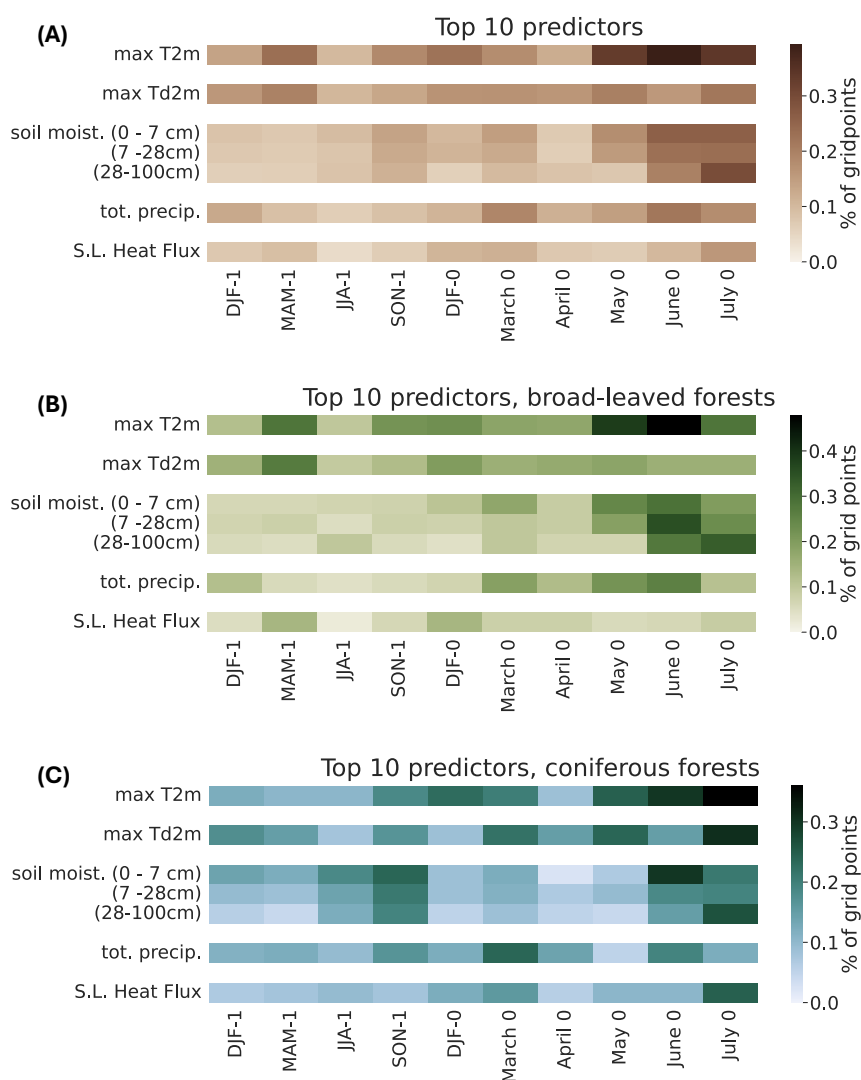
Figure 3. Importance of the predictors for all forest gridpoints. Each cell represents one predictor, i.e. a given variable (y-axis) at a specific time period (x-axis). The color shading of each cell indicates the percentage of gridpoints where this predictor ranks among the top 10 most important predictors in the random forest model. The percentage is calculated for (A) all forest gridpoints over Europe, (B) broad-leaved forest gridpoints only, and (C) coniferous forest gridpoints only.
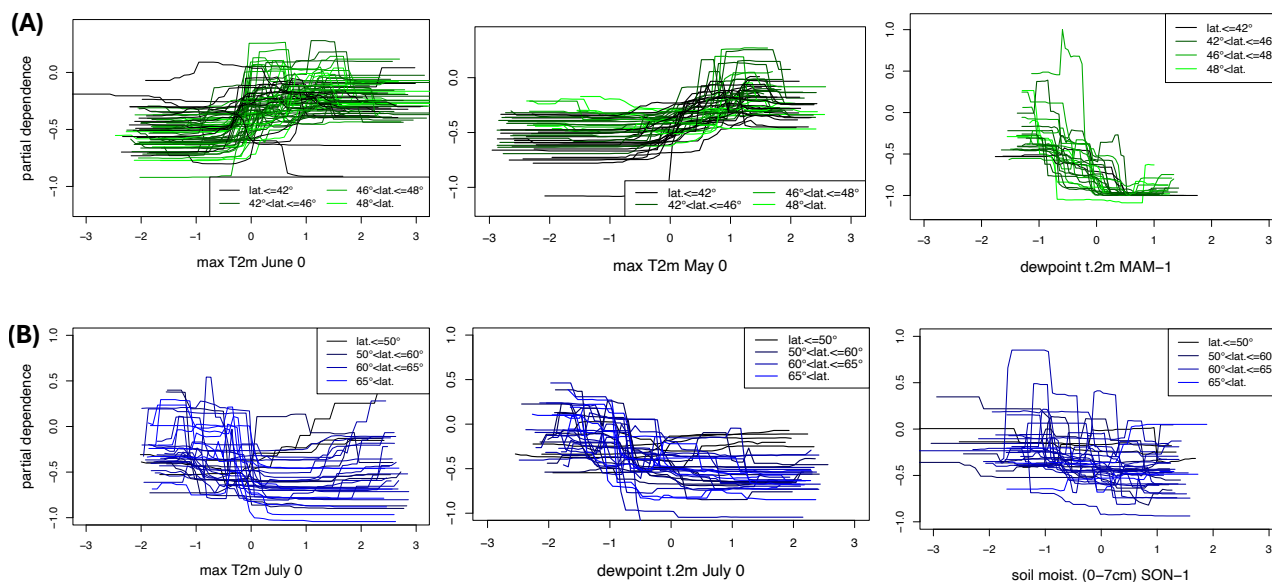
Figure 4. Partial dependence of forest damage (y-axis) with a given predictor anomalies (x-axis), for broad-leaved forest (A) and coniferous forest (B). The predictors are (A) maximum 2-m temperature in June and May of the same year, and maximum dewpoint temperature in spring of the preceding year, for broad-leaved forests only and (B) maximum 2-m temperature and dewpoint temperature in July of the same year, and soil moisture (0-7 cm depth) in autumn of the preceding year, for coniferous forests only. The color shade indicates the latitude. For each dependence plot, we display only the gridpoints for which the predictor is one of the top 10 predictors.

5 Discussion

5.1 Identified adverse conditions

Our model identified dry and hot conditions as adverse conditions for European broad-leaved forests, i.e. high temperature and low dew-point temperature, agreeing with existing literature (Rita et al., 2019; Beloiu et al., 2022; Rubio-Cuadrado et al., 2018;

275   Senf et al., 2020). Broad-leaved forests are predominantly located in the central and southern part of Europe (Fig. D1), often water-limited, with an increasing trend of drought frequency (Vicente-Serrano et al., 2014; Gudmundsson and Seneviratne, 2016; Rita et al., 2019).

     The observed link between dry conditions and increased coniferous forest damage probability (dew point in July of the same year and soil moisture in the preceding year) is consistent with existing literature, which highlights drought stress as a factor

280   for bark beetle infestations (Dobbertin et al., 2007; Müller et al., 2022). The link between July temperature and coniferous forest browning is rather heterogeneous over Europe. For low latitudes grid points, the association between forest damage and warm July temperature aligns with the fact that dry and hot conditions are adverse conditions (Senf et al., 2020; Müller et al.,

2022). For high latitudes coniferous forests, a possible explanation for the association between cold July temperatures and low greenness could be that Northern Europe is energy-limited (see Fig. 1 in McVicar et al., 2012).

285   We established a statistical link between the preceding seasonal conditions and forest damage during the following year, hinting towards a source of inter-annual predictability for European forests. Indeed, forests impacted by extreme summer conditions are more vulnerable to adverse conditions the following year Brun et al. (2020); Frei et al. (2022). Consecutive years with adverse conditions may reduce tree resilience, reflecting a "memory effect" (Anderegg et al., 2015; Hermann et al., 2023). A causality analysis (Peters et al., 2017) could explore the role of previous summers' forest state as a predictor, although
290   this framework is beyond the scope of our study.

    As an initial criterion, we aimed to include relevant variables from S2S forecast model output, so that our results may be used subsequently to use S2S forecasts for prediction. While vapor-pressure deficit (VPD) can significantly impact trees by reducing stomatal conductance and photosynthesis (Grossiord et al., 2020; McDowell et al., 2022; Schoenbeck et al., 2022), this variable is unavailable in S2S forecasts. We therefore chose dew-point temperature to measure the water content in the air.

295   We excluded soil temperature, as its variability is driven by air temperature, which is already a predictor in our model. We also discarded snow water equivalent for a better comparison between regions, as this variable may be relevant only in snowmelt-driven catchments. We hypothesize that the precipitation and temperature contain the information that snow water equivalent would bring. We did not consider wind storms, focusing on long-term, large-scale forest damage. Storm damage, though potentially extreme, is more localized (Hermann et al., 2023) and should be assessed with higher resolution NDVI
300   datasets (Giannetti et al., 2021).

5.2   Technical details

As CORINE land cover maps are only available from 1990, we used a static forest mask for the whole NDVI time series (EEA, 2020, Corine Land Cover 2018). At least between 1990 and 2006, most areas in Europe exhibit stable or slightly increasing forestland Kuemmerle et al. (2016). We hypothesize that the changes in forest cover do not substantially influence
305   the identification of large-scale damages as identified in our analysis

    AVHRR data has a medium spatial resolution (1.1 km at nadir) and does not capture the fine vegetation variability. Higher resolution datasets can better capture high-resolution vegetation dynamics (Benson et al., 2024; Kladny et al., 2024), but have a lower temporal resolution. We chose AVHRR data as a tradeoff between long temporal availability and spatial resolution, emphasizing that the identified forest damage are large-scale anomalies (on a $0.1°$ grid).
310   Soil moisture is challenging in reanalysis datasets due to sparse and varied measurement points and soil types. Nonetheless, Zheng et al. (2024) shows that ERA5-Land soil moisture is one of the most reliable reanalysis products and correlates well with observations. We use reanalysis to ensure consistency with the other ERA5 variables and we compute soil moisture anomalies to reduce systematic bias uncertainty.

    Overall, while these choices may influence the performance of the RF, its high predictive accuracy substantially reduces the
315   concern regarding their impact.

6 Conclusions

In this study, we provided an automated procedure to pinpoint relevant hydro-meteorological drivers for forest damage over Europe. We used the AVHRR NDVI data, which spans a temporal range of 41 years, to capture the state of European forests during summer. We used the fine spatial resolution of the AVHRR data to create a sufficiently long time series for conducting a random forest (RF) classification. The RF model is run individually for all $0.5° \times 0.5°$ forest gridpoints in Europe and demonstrates strong predictive performance for identifying low-greenness events during summer based on prior hydro-meteorological conditions. The high CSI indicates that given a cutoff level (that assigns a probability of damage to a "0" or a "1"), the model accurately predicts low-greenness events more often than missing an extreme or producing a false alarm. The high AUC indicates that the performance does not depend on the cut-off level. Our model demonstrates a high predictive score and is sufficiently general to compare the link between drivers and forest damage across all grid points in Europe.

We show that the most essential time periods are primarily spring and early summer preceding the studied summer. Temperature and soil moisture conditions in spring and early summer are the most important predictors of European summer forest damage. Temperature, dew-point temperature, and soil moisture in the preceding year also play a role, indicating a multi-year impact of hydro-meteorological conditions. The identified important predictors in Europe are mainly related to dry and hot conditions, especially for broad-leaved forests or low latitudes coniferous forests. However, coniferous forests exhibit more heterogeneous and non-linear relationships between hydro-meteorological predictors and summer low forest greenness events.

The crucial conditions and time-periods are identified locally and all the hydro-meteorological variables considered here are available as sub-seasonal to seasonal forecast products. Therefore, regional forest management organizations can use our method findings to anticipate and plan preventive measures. Such preventive measures would mitigate the economic and environmental costs of forest damage.

Code and data availability. ERA5 and ERA5 land data are publicly available (https://confluence.ecmwf.int/display/CKB/How+to+download+ ERA5). The AVHRR NDVI data can be accessed on the following link: https://doi.org/10.48620/400. The codes and data supporting the findings of this study will be made publicly available on Githib upon acceptance for publication. Reviewers may request access to the codes and data prior to publication.

340 **Author contribution**

PR, DD, AG, and PV conceptualized the study. SD curated the NDVI data. PR designed the methodology and performed the study's formal analysis, validation, and visualization. PR wrote the manuscript draft; DD, SD, AD, and PV reviewed and edited the manuscript.

Competing interests

345 The authors declare that they have no conflict of interest.

Acknowledgements. PR expresses her gratitude to Dr. Andries De Vries for downloading the ERA5 data, Dr. Marj Tonini for her assistance with the Random Forest model, and Prof. Elizabeth Barnes for the fruitful discussions regarding the stacking procedure. PR is also thankful to Dr. Lukas Gudmundsson for his insights on soil moisture, Dr. Mauro Hermann for the nice discussion regarding low greenness events, and to Prof. Charlotte Grossiord and Dr. Thomas Wohlgemuth for their insights on plant physiology.

350 All the statistical analysis where performed with R (linear detrending with package `pracma`, LASSO regression with package `glmnet`, random forest with package `randomForest`)

PR is grateful for the Early Career Postdoctoral Fellowship awarded by the Faculty of Geosciences and the Environment at the University of Lausanne. This project has received funding from the European Research Council (ERC) under the European Union's Horizon 2020 research and innovation programme (grant agreement No. 847456). Support from the Swiss National Science Foundation through project 355 PP00P2_198896 to DD is gratefully acknowledged. SD expresses her gratitude to the Dr. Alfred Bretscher Stipendium for climate and air pollution research of the University of Bern.

Appendix A: Quality control of the AVHRR NDVI composites
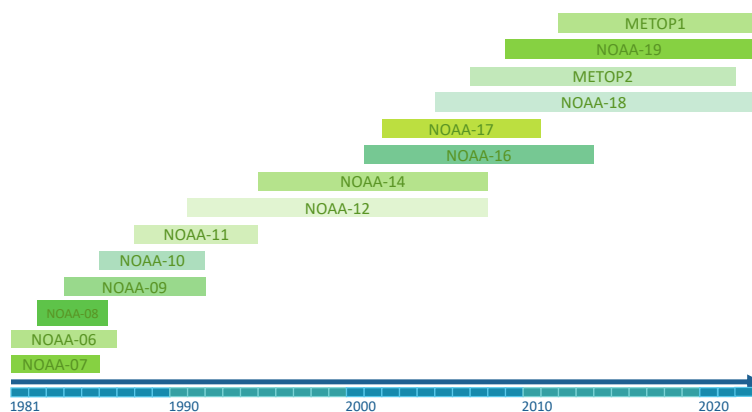
Figure A1. List of the satellites used for our study and the years for which they are available (x-axis)

The 10-day AVHRR NDVI dataset Dupuis et al., 2024, hosted at the University of Bern has been derived by computing the median NDVI valued across ten consecutive days. Prior to the compositing, a cloud mask is applied to the single satellite image to filter out pixels contaminated by clouds. Each pixel in the AVHRR dataset was subject to quality control before computing the 10-day composites from the daily NDVI data. For a given observation, the pixel is masked out if the satellite viewing angle is higher than $55°$. Additionally, the sun zenith angle must be below $80°$ for the observation to be valid. Similarly, if the cloud probability mask is above 30 % or the quality of the cloud mask is not qualified as 'good', then the pixel is masked out. We then compute the 10-day composite as the mean NDVI value for the valid days over the 10 days. The number of valid pixels used for the compositing generating is recorded, as well as the number of pixels exhibiting cloud probabilities between 1% and 30%. If less than two valid days are valid for a given 10-composites, the composite is set to missing data.

Appendix B: Forest damage
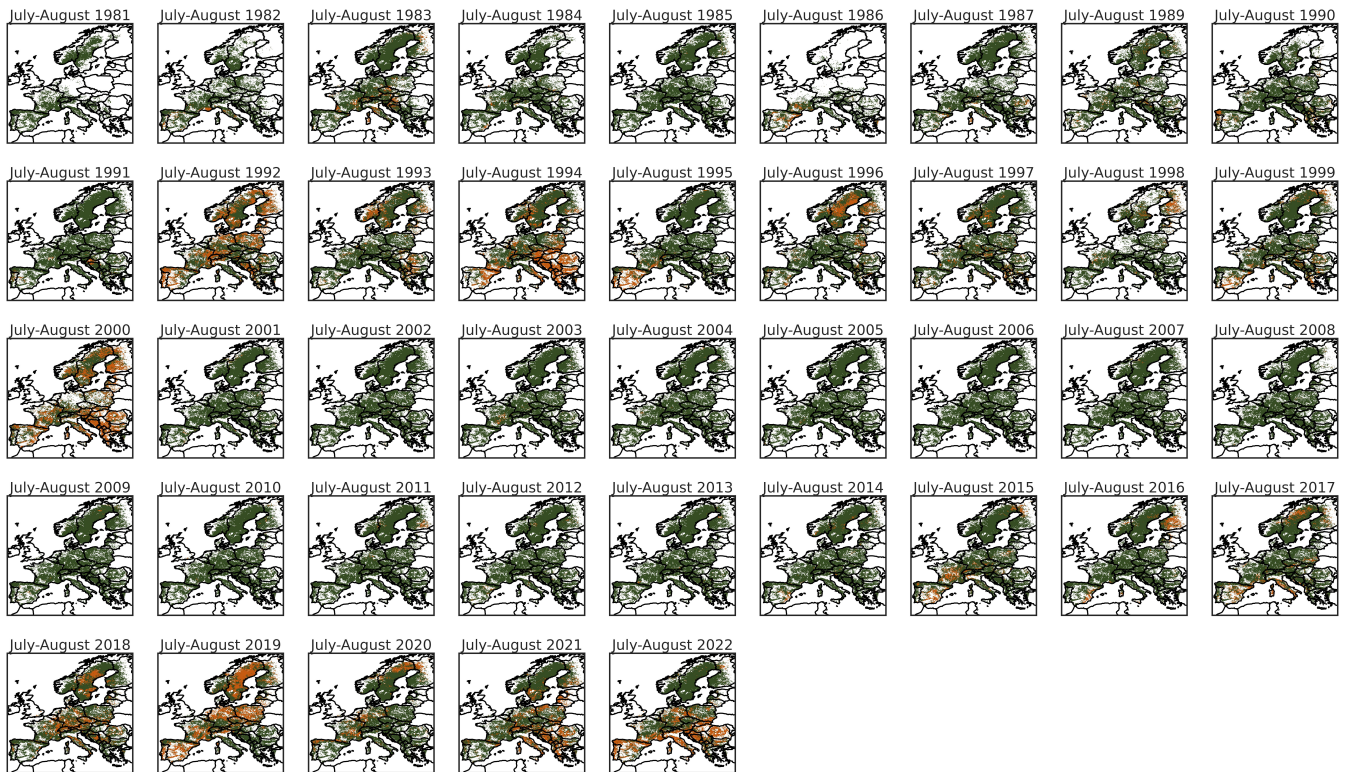
Figure B1. Time series of forest damage on a $0.1°\times0.1°$ grid, as defined in Section 2.2. A forest gridpoint is displayed in orange if it experiences a low-greeness event ($Y_t = 1$, in Sec. 2.2), and in green for normal years ($Y_t = 0$, in Sec. 2.2).
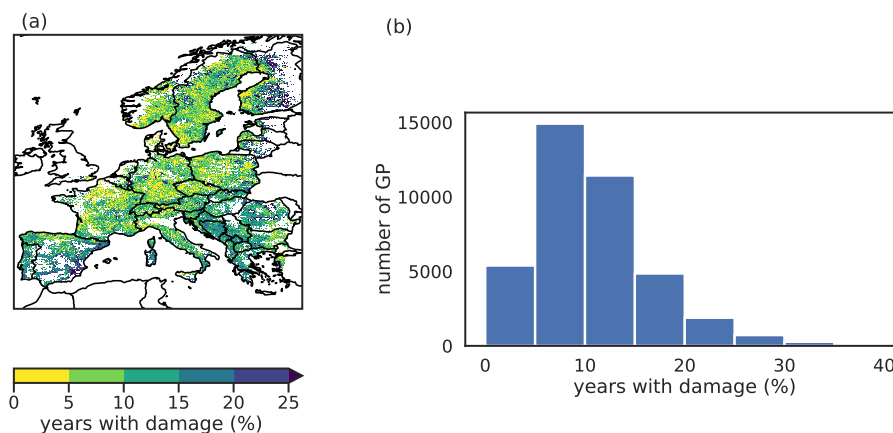
Figure B2. (a) Spatial representation and (b) histogram (GP = gridpoint) of the percentage of years with damage on the forest for the 0.1°
grid, as defined in Section 2.2.

Appendix C: Data processing
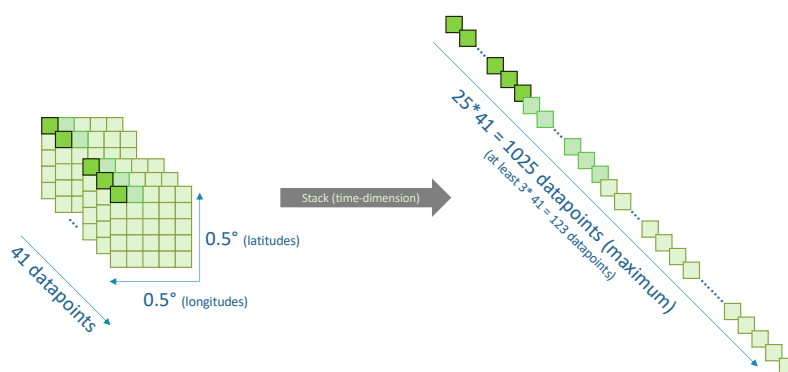
Figure C1. Stacking procedure to obtain longer time series. All of the 0.1×0.1 forest GPs in a 0.5×0.5 box are stacked in time. The same
procedure is applied for the preceding hydro-meteorological conditions, individually for each GP.

Appendix D: Forest Type
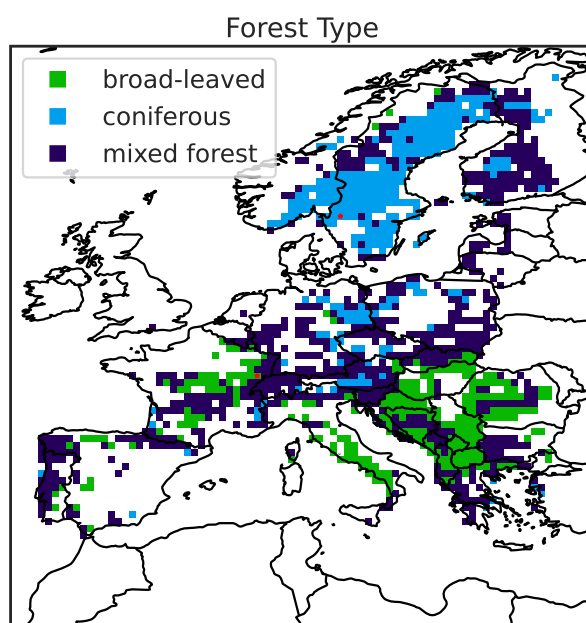
Figure D1. Forest type on the grid of the random forest model's output ($0.1° \times 0.1°$ grid). The random forest model was run on 1248 gridpoints in total, among which 263 of them are broad-leaved forest gridpoints and 303 of them are coniferous forest gridpoints. The two red stars indicate the location of the two gridpoints studied in Fig. 2.

370 **References**

Adams, H. D., Zeppel, M. J. B., Anderegg, W. R. L., Hartmann, H., Landhäusser, S. M., Tissue, D. T., et al.: A multi-species synthesis of physiological mechanisms in drought-induced tree mortality, Nature Ecology & Evolution, 1, 1285–1291, https://doi.org/10.1038/s41559-017-0248-x, 2017.

Alavi, G.: The impact of soil moisture on stem growth of spruce forest during a 22-year period, Forest Ecology and Management, 166, 17–33,
375   https://doi.org/https://doi.org/10.1016/S0378-1127(01)00661-2, 2002.

Anderegg, W. R. L., Schwalm, C., Biondi, F., Camarero, J. J., Koch, G., Litvak, M., Ogle, K., Shaw, J. D., Shevliakova, E., Williams, A. P., Wolf, A., Ziaco, E., and Pacala, S.: Pervasive drought legacies in forest ecosystems and their implications for carbon cycle models, Science, 349, 528–532, https://doi.org/10.1126/science.aab1833, 2015.

Bannari, A., Morin, D., Bonn, F., and Huete, A. R.: A review of vegetation indices, Remote Sensing Reviews, 13, 95–120,
380   https://doi.org/10.1080/02757259509532298, 1995.

Barben, M., Wunderle, S., and Dupuis, S.: A 40-Year Time Series of Land Surface Emissivity Derived from AVHRR Sensors: A Fennoscandian Perspective, Remote Sensing, 16, 3686, https://doi.org/10.3390/rs16193686, 2024.

Bastos, A., Ciais, P., Park, T., Zscheischler, J., Yue, C., Barichivich, J., Myneni, R. B., Peng, S., Piao, S., and Zhu, Z.: Was the extreme Northern Hemisphere greening in 2015 predictable?, Environmental Research Letters, 12, 044 016, https://doi.org/10.1088/1748-9326/aa67b5,
385   2017.

Beloiu, M., Stahlmann, R., and Beierkuhnlein, C.: Drought impacts in forest canopy and deciduous tree saplings in Central European forests, Forest Ecology and Management, 509, 120 075, https://doi.org/10.1016/j.foreco.2022.120075, 2022.

Benson, V., Robin, C., Requena-Mesa, C., Alonso, L., Carvalhais, N., Cortés, J., Gao, Z., Linscheid, N., Weynants, M., and Reichstein, M.: Multi-modal Learning for Geospatial Vegetation Forecasting, in: Proceedings of the IEEE/CVF Conference on Computer Vision and
390   Pattern Recognition (CVPR), pp. 27 788–27 799, 2024.

Breiman, L.: Random Forests, Machine Learning, 45, 5–32, https://doi.org/10.1023/A:1010933404324, 2001.

Brodribb, T. J., Powers, J., Cochard, H., and Choat, B.: Hanging by a thread? Forests and drought, Science, 368, 261–266, https://doi.org/10.1126/science.aat7631, 2020.

Brun, P., Psomas, A., Ginzler, C., Thuiller, W., Zappa, M., and Zimmermann, N. E.: Large-scale early-wilting response of Central European
395   forests to the 2018 extreme drought, Global Change Biology, 26, 7021–7035, https://doi.org/10.1111/gcb.15360, 2020.

Buras, A., Rammig, A., and Zang, C. S.: The European Forest Condition Monitor: Using Remotely Sensed Forest Greenness to Identify Hot Spots of Forest Decline, Frontiers in Plant Science, 12, https://doi.org/10.3389/fpls.2021.689220, 2021.

Choler, P., Bayle, A., Carlson, B. Z., Randin, C., Filippa, G., and Cremonese, E.: The tempo of greening in the European Alps: Spatial variations on a common theme, Global Change Biology, 27, 5614–5628, https://doi.org/10.1111/gcb.15820, 2021.

400 Didan, K.: MOD13Q1 MODIS/Terra Vegetation In- dices 16-Day L3 Global 250m SIN Grid V006, https://doi.org/https://doi.org/10.5067/MODIS/MOD13Q1.006, 2015.

Dobbertin, M., Wermelinger, B., Bigler, C., Bürgi, M., Carron, M., Forster, B., Gimmi, U., and Rigling, A.: Linking Increasing Drought Stress to Scots Pine Mortality and Bark Beetle Infestations, The Scientific World JOURNAL, 7, 231–239, https://doi.org/10.1100/tsw.2007.58, 2007.

405   Domeisen, D. I., White, C. J., Afargan-Gerstman, H., Muñoz, Á. G., Janiga, M. A., Vitart, F., Wulff, C. O., Antoine, S., Ardilouze, C., Batté, L., et al.: Advances in the subseasonal prediction of extreme events: Relevant case studies across the globe, Bulletin of the American Meteorological Society, 103, E1473–E1501, 2022.

Dupuis, S., Rivoire, P., Barben, M., and Wunderle, S.: 40-year AVHRR top-of-atmosphere NDVI dataset, https://doi.org/10.48620/400, 2024.

EEA: CORINE Land Cover 2018 (vector), Europe, 6-yearly - version 2020 20u1, https://doi.org/10.2909/
410   71c95a07-e296-44fc-b22b-415f42acfdf0, 2020.

FAO: Global Forest Resources Assessment 2020: Main report, Rome, https://doi.org/https://doi.org/10.4060/ca9825en, 2020.

Ferreira, A. J. D., Alegre, S. P., Coelho, C. O. A., Shakesby, R. A., Páscoa, F. M., Ferreira, C. S. S., Keizer, J. J., and Ritsema, C.: Strategies to prevent forest fires and techniques to reverse degradation processes in burned areas, CATENA, 128, 224–237, https://doi.org/https://doi.org/10.1016/j.catena.2014.09.002, 2015.

415   Fontana, F. M., Trishchenko, A. P., Khlopenkov, K. V., Luo, Y., and Wunderle, S.: Impact of orthorectification and spatial sampling on maximum NDVI composite data in mountain regions, Remote Sensing of Environment, 113, 2701–2712, https://doi.org/https://doi.org/10.1016/j.rse.2009.08.008, 2009.

Frei, E. R., Gossner, M. M., Vitasse, Y., Queloz, V., Dubach, V., Gessler, A., Ginzler, C., Hagedorn, F., Meusburger, K., Moor, M., Samblás Vives, E., Rigling, A., Uitentuis, I., von Arx, G., and Wohlgemuth, T.: European beech dieback after premature leaf senescence during
420   the 2018 drought in northern Switzerland, Plant Biology, 24, 1132–1145, https://doi.org/https://doi.org/10.1111/plb.13467, 2022.

Friedman, J. H.: Greedy function approximation: A gradient boosting machine, The Annals of Statistics, 29, 1189–1232, https://doi.org/10.1214/aos/1013203451, 2001.

Giannetti, F., Pecchi, M., Travaglini, D., Francini, S., D'Amico, G., Vangi, E., Cocozza, C., and Chirici, G.: Estimating VAIA Windstorm Damaged Forest Area in Italy Using Time Series Sentinel-2 Imagery and Continuous Change Detection Algorithms, Forests, 12,
425   https://doi.org/10.3390/f12060680, 2021.

Grossiord, C., Buckley, T. N., Cernusak, L. A., Novick, K. A., Poulter, B., Siegwolf, R. T. W., Sperry, J. S., and McDowell, N. G.: Plant responses to rising vapor pressure deficit, New Phytologist, 226, 1550–1566, https://doi.org/10.1111/nph.16485, 2020.

Gudmundsson, L. and Seneviratne, S. I.: Anthropogenic climate change affects meteorological drought risk in Europe, Environmental Research Letters, 11, 044 005, https://doi.org/10.1088/1748-9326/11/4/044005, 2016.

430   Hermann, M., Röthlisberger, M., Gessler, A., Rigling, A., Senf, C., Wohlgemuth, T., and Wernli, H.: Meteorological history of low-forest-greenness events in Europe in 2002–2022, Biogeosciences, 20, 1155–1180, https://doi.org/10.5194/bg-20-1155-2023, 2023.

Hersbach, H., Bell, B., Berrisford, P., Horányi, A., Sabater, J. M., Nicolas, J., Radu, R., Schepers, D., Simmons, A., Soci, C., and Dee, D.: Global reanalysis: goodbye ERA-Interim, hello ERA5, ECMWF Newsletter, 146, 17–24, https://doi.org/10.21957/vf291hehd7, 2019.

Hinckley, T. M., Dougherty, P. M., Lassoie, J. P., Roberts, J. E., and Teskey, R. O.: A Severe Drought: Impact on Tree Growth, Phenology, Net
435   Photosynthetic Rate and Water Relations, The American Midland Naturalist, 102, 307–316, http://www.jstor.org/stable/2424658, 1979.

IPCC: Summary for Policymakers [H.-O. Pörtner, D.C. Roberts, E.S. Poloczanska, K. Mintenbeck, M. Tignor, A. Alegrìa, M. Craig, S. Langsdorf, S. Löschke, V. Möller, A. Okem (eds.)]. In: Climate Change 2022: Impacts, Adaptation, and Vulnerability. Contribution of Working Group II to the Sixth Assessment Report of the Intergovernmental Panel on Climate Change [H.-O. Pörtner, D.C. Roberts, M. Tignor, E.S. Poloczanska, K. Mintenbeck, A. Alegrà, M. Craig, S. Langsdorf, S. Löschke, V. Möller, A. Okem, B. Rama (eds.)], pp. 3–33,
440   https://doi.org/doi:10.1017/9781009325844.001, 2022.

Jan Weslien, Öhrn, P., Rosenberg, O., and Schroeder, M.: Effects of sanitation logging in winter on the Eurasian spruce bark beetle and predatory long-legged flies, Forest Ecology and Management, 554, 121 665, https://doi.org/https://doi.org/10.1016/j.foreco.2023.121665, 2024.

Jenkins, M. and Schaap, B.: Forest Ecosystem Services, UNFF13 Background Analytical Study, 1, 1–50, https://www.un.org/esa/forests/wp-content/uploads/2018/05/UNFF13_BkgdStudy_ForestsEcoServices.pdf, last accessed: 7 October 2024, 2018.

John Nay, E. B. and Gilligan, J.: A machine-learning approach to forecasting remotely sensed vegetation health, International Journal of Remote Sensing, 39, 1800–1816, https://doi.org/10.1080/01431161.2017.1410296, 2018.

Kladny, K.-R., Milanta, M., Mraz, O., Hufkens, K., and Stocker, B. D.: Enhanced prediction of vegetation responses to extreme drought using deep learning and Earth observation data, Ecological Informatics, 80, 102 474, https://doi.org/https://doi.org/10.1016/j.ecoinf.2024.102474, 2024.

Kriegler, F. J., Malila, W. A., Nalepka, R. F., and Richardson, W.: Preprocessing transformations and their effects on multispectral recognition, in: Proceedings of the Sixth International Symposium on Remote Sensing of Environment, pp. 97–131, University of Michigan, Ann Arbor, 1969.

Kuemmerle, T., Levers, C., Erb, K., Estel, S., Jepsen, M. R., Müller, D., Plutzar, C., Stürck, J., Verkerk, P. J., Verburg, P. H., and Reenberg, A.: Hotspots of land use change in Europe, Environmental Research Letters, 11, 064 020, https://doi.org/10.1088/1748-9326/11/6/064020, 2016.

Leuschner, C. and Ellenberg, H.: Vegetation Ecology of Central Europe: Volume I: Ecology of Central European Forests, Springer Berlin Heidelberg, New York, NY, ISBN 978-3-319-43042-3, https://doi.org/10.1007/978-3-319-43042-3, 2017.

Lindner, M., Fitzgerald, J. B., Zimmermann, N. E., Reyer, C., Delzon, S., van der Maaten, E., Schelhaas, M.-J., Lasch, P., Eggers, J., van der Maaten-Theunissen, M., Suckow, F., Psomas, A., Poulter, B., and Hanewinkel, M.: Climate change and European forests: what do we know, what are the uncertainties, and what are the implications for forest management?, Journal of Environmental Management, 146, 69–83, https://doi.org/10.1016/j.jenvman.2014.07.030, 2014.

Mariën, B., Dox, I., De Boeck, H. J., Willems, P., Leys, S., Papadimitriou, D., and Campioli, M.: Does drought advance the onset of autumn leaf senescence in temperate deciduous forest trees?, Biogeosciences, 18, 3309–3330, https://doi.org/10.5194/bg-18-3309-2021, 2021.

McDowell, N. G., Sapes, G., Pivovaroff, A., Adams, H. D., Allen, C. D., Anderegg, W. R. L., Arend, M., Breshears, D. D., Brodribb, T., Choat, B., Cochard, H., Cáceres, M. D., Kauwe, M. G. D., Grossiord, C., Hammond, W. M., Hartmann, H., Hoch, G., Kahmen, A., Klein, T., Mackay, D. S., Mantova, M., Martínez-Vilalta, J., Medlyn, B. E., Mencuccini, M., Nardini, A., Oliveira, R. S., Sala, A., Tissue, D. T., Torres-Ruiz, J. M., Trowbridge, A. M., Trugman, A. T., Wiley, E., and Xu, C.: Mechanisms of woody-plant mortality under rising drought, CO_2 and vapour pressure deficit, Nature Reviews Earth & Environment, 3, 294–308, https://doi.org/10.1038/s43017-022-00272-1, 2022.

McVicar, T. R., Roderick, M. L., Donohue, R. J., Li, L. T., Niel, T. G. V., Thomas, A., Grieser, J., Jhajharia, D., Himri, Y., Mahowald, N. M., Mescherskaya, A. V., Kruger, A. C., Rehman, S., and Dinpashoh, Y.: Global review and synthesis of trends in observed terrestrial near-surface wind speeds: Implications for evaporation, Journal of Hydrology, 416-417, 182–205, https://doi.org/10.1016/j.jhydrol.2011.10.024, 2012.

Meier, M., Vitasse, Y., Bugmann, H., and Bigler, C.: Phenological shifts induced by climate change amplify drought for broad-leaved trees at low elevations in Switzerland, Agricultural and Forest Meteorology, 307, 108 485, https://doi.org/10.1016/j.agrformet.2021.108485, 2021.

Muñoz-Sabater, J., Dutra, E., Agustí-Panareda, A., Albergel, C., Arduini, G., Balsamo, G., Boussetta, S., Choulga, M., Harrigan, S., Hersbach, H., Martens, B., Miralles, D. G., Piles, M., Rodríguez-Fernández, N. J., Zsoter, E., Buontempo, C., and Thépaut, J. N.: ERA5-Land:

A state-of-the-art global reanalysis dataset for land applications, Earth System Science Data, 13, 4349–4383, https://doi.org/10.5194/essd-13-4349-2021, 2021.

480 Müller, M., Olsson, P.-O., Eklundh, L., Jamali, S., and Ardö, J.: Features predisposing forest to bark beetle outbreaks and their dynamics during drought, Forest Ecology and Management, 523, 120 480, https://doi.org/10.1016/j.foreco.2022.120480, 2022.

Ozenda, P.: Végétation du continent européen, Delachaux et Niestlé, Paris, ISBN 2603009540, 1994.

Peters, J., Janzing, D., and Schölkopf, B.: Elements of Causal Inference: Foundations and Learning Algorithms, MIT Press, Cambridge, MA, USA, 2017.

485 Pettorelli, N., Vik, J. O., Mysterud, A., Gaillard, J. M., Tucker, C. J., and Stenseth, N. C.: Using the satellite-derived NDVI to assess ecological responses to environmental change, Trends in Ecology and Evolution, 20, 503–510, https://doi.org/10.1016/j.tree.2005.05.011, 2005.

Pureswaran, D. S., Roques, A., and Battisti, A.: Forest Insects and Climate Change, Current Forestry Reports, 4, 35–50, https://doi.org/10.1007/s40725-018-0075-6, 2018.

RDocumentation: partialPlot function, https://www.rdocumentation.org/packages/randomForest/versions/4.7-1.1/topics/partialPlot, accessed: 2024-10-07, 2024.

490 Rita, A., Brunetti, M., Nolè, A., Serio, C., Borghetti, M., Vicente-Serrano, S. M., Tramutoli, V., Camarero, J. J., Pergola, N., and Ripullone, F.: The impact of drought spells on forests depends on site conditions: The case of 2017 summer heat wave in southern Europe, Global Change Biology, 26, 851–863, https://doi.org/10.1111/gcb.14825, 2019.

Rouse, J. W., Haas, R. H., Schell, J. A., and Deering, D. W.: Monitoring vegetation systems in the great plains with ERTS, in: Third Earth
495 Resources Technology Satellite-1 Symposium- Volume I: Technical Presentations, edited by Freden, S. C., Mercanti, E. P., and Becker, M. A., p. 309, NASA, Washington, DC, 1974.

Rubio-Cuadrado, Á., Camarero, J. J., del Río, M., Sánchez-González, M., Ruiz-Peinado, R., Bravo-Oviedo, A., Gil, L., and Montes, F.: Long-term impacts of drought on growth and forest dynamics in a temperate beech-oak-birch forest, Agricultural and Forest Meteorology, 259, 48–59, https://doi.org/10.1016/j.agrformet.2018.04.015, 2018.

500 Rumpf, S. B., Gravey, M., Brönnimann, O., Luoto, M., Cianfrani, C., Mariethoz, G., and Guisan, A.: From white to green: Snow cover loss and increased vegetation productivity in the European Alps, Science, 376, 1119–1122, https://doi.org/10.1126/science.abn6697, 2022.

Schaefer, J. T.: The Critical Success Index as an Indicator of Warning Skill, Weather and Forecasting, 5, 570–575, https://doi.org/10.1175/1520-0434(1990)005<0570:TCSIAA>2.0.CO;2, 1990.

Schoenbeck, L. C., Schuler, P., Lehmann, M. M., Mas, E., Mekarni, L., Pivovaroff, A. L., Turberg, P., and Grossiord, C.: Increasing temper-
505 ature and vapour pressure deficit lead to hydraulic damages in the absence of soil drought, Plant, Cell & Environment, 45, 3275–3289, https://doi.org/10.1111/pce.14425, 2022.

Senf, C., Buras, A., Zang, C. S., Rammig, A., and Seidl, R.: Excess forest mortality is consistently linked to drought across Europe, Nature Communications, 11, 6200, https://doi.org/10.1038/s41467-020-19924-1, 2020.

Sperlich, D., Chang, C., Peñuelas, J., Gracia, C., and Sabaté, S.: Seasonal variability of foliar photosynthetic and morphological traits and
510 drought impacts in a Mediterranean mixed forest, Tree Physiology, 35, 501–520, https://doi.org/10.1093/treephys/tpv017, 2015.

Swets, J. A.: Measuring the accuracy of diagnostic systems, Science, 240, 1285–1293, https://doi.org/10.1126/science.3287615, 1988.

Tibshirani, R.: Regression Shrinkage and Selection via the Lasso, Journal of the Royal Statistical Society. Series B (Methodological), 58, 267–288, http://www.jstor.org/stable/2346178, 1996.

Trishchenko, A. P.: Effects of spectral response function on surface reflectance and NDVI measured with moderate resolution satellite sensors: Extension to AVHRR NOAA-17, 18 and METOP-A, Remote Sensing of Environment, 113, 335–341, https://doi.org/10.1016/j.rse.2008.10.002, 2009.

Trishchenko, A. P., Cihlar, J., and Li, Z.: Effects of spectral response function on surface reflectance and NDVI measured with moderate resolution satellite sensors, Remote Sensing of Environment, 81, 1–18, https://doi.org/10.1016/S0034-4257(01)00328-5, 2002.

Vicente-Serrano, S. M., Lopez-Moreno, J.-I., Beguería, S., Lorenzo-Lacruz, J., Sanchez-Lorenzo, A., García-Ruiz, J. M., Azorin-Molina, C., Morán-Tejeda, E., Revuelto, J., Trigo, R., Coelho, F., and Espejo, F.: Evidence of increasing drought severity caused by temperature rise in southern Europe, Environmental Research Letters, 9, 044 001, https://doi.org/10.1088/1748-9326/9/4/044001, 2014.

Vogel, J., Rivoire, P., Deidda, C., Rahimi, L., Sauter, C. A., Tschumi, E., Wiel, K. V. D., Zhang, T., and Zscheischler, J.: Identifying meteorological drivers of extreme impacts: An application to simulated crop yields, Earth System Dynamics, 12, 151–172, https://doi.org/10.5194/esd-12-151-2021, 2021.

Weber, H., Naegeli, K., and Wunderle, S.: Impact of Forest Canopy Parameterization on Space-Borne Snow on Ground Detection, in: 2021 IEEE International Geoscience and Remote Sensing Symposium IGARSS, pp. 864–867, https://doi.org/10.1109/IGARSS47720.2021.9553397, 2021.

White, C. J., Domeisen, D. I., Acharya, N., Adefisan, E. A., Anderson, M. L., Aura, S., Balogun, A. A., Bertram, D., Bluhm, S., Brayshaw, D. J., et al.: Advances in the application and utility of subseasonal-to-seasonal predictions, Bulletin of the American Meteorological Society, 103, E1448–E1472, 2022.

Young, D. J. N., Stevens, J. T., Earles, J. M., Moore, J., Ellis, A., Jirka, A. L., and Latimer, A. M.: Long-term climate and competition explain forest mortality patterns under extreme drought, Ecology Letters, 20, 78–86, https://doi.org/https://doi.org/10.1111/ele.12711, 2017.

Zeng, Y., Hao, D., Huete, A., Dechant, B., Berry, J., Chen, J. M., Joiner, J., Frankenberg, C., Bond-Lamberty, B., Ryu, Y., Xiao, J., Asrar, G. R., and Chen, M.: Optical vegetation indices for monitoring terrestrial ecosystems globally, Nature Reviews Earth & Environment, 3, 477–491, https://doi.org/10.1038/s43017-022-00298-5, 2022.

Zheng, Y., Coxon, G., Woods, R., Power, D., Rico-Ramirez, M. A., McJannet, D., Rosolem, R., Li, J., and Feng, P.: Evaluation of reanalysis soil moisture products using cosmic ray neutron sensor observations across the globe, Hydrology and Earth System Sciences, 28, 1999–2022, https://doi.org/10.5194/hess-28-1999-2024, 2024.

Zhou, L., Kaufmann, R. K., Tian, Y., Myneni, R. B., and Tucker, C. J.: Relation between interannual variations in satellite measures of northern forest greenness and climate between 1982 and 1999, Journal of Geophysical Research: Atmospheres, 108, ACL 3–1–ACL 3–16, https://doi.org/https://doi.org/10.1029/2002JD002510, 2003.